Journal of Nanoparticle Research (2005) 7: 507–516
DOI 10.1007/s11051-005-5133-x

Modeling and simulation of ionic currents in three-dimensional microfluidic devices with nanofluidic interconnects

Aveek N. Chatterjee, Donald M. Cannon Jr., Enid N. Gatimu, Jonathan V. Sweedler, Narayana R. Aluru and Paul W. Bohn*
*Department of Chemistry, Department of Mechanical & Industrial Engineering and the Beckman Institute for Advanced Science and Technology, 405 N. Mathews Ave., Urbana, IL 61801, USA; *Author for correspondence (E-mail: bohn@scs.uiuc.edu)*

Received 5 April 2005; accepted in revised form 6 April 2005

Key words: nanofluidics, modeling, simulation, molecular gate, three-dimensional architecture, nanotechnology, water quality

Abstract

Electrokinetic fluid flow in nanocapillary array (NCA) membranes between vertically separated microfluidic channels offers an attractive alternative to using mechanical action to achieve fluidic communication between different regions of lab-on-a-chip devices. By adjusting the channel diameter, a, and the inverse Debye length, κ, and applying the appropriate external potential, the nanochannel arrays, can be made to behave like digital fluidic switches, and the movement of molecules from one side of the array to the other side can be controlled. However, inherent differences in ionic mobility lead to non-equilibrium ion populations on the downstream side, which, in turn, shows up through transient changes in the microchannel conductance. Here we describe coupled calculations and experiments in which the electrical properties of a microfluidic–nanofluidic hybrid architecture are simulated by a combination of a compact model for the bulk electrical properties and iterative self-consistent solutions of the coupled Poisson, Nernst–Planck, and Navier–Stokes equations to recover the detailed ion motion in the nanopores. The transient electrical conductivity in the microchannel, after application of a forward bias pulse to the NCA membrane, is recovered in quantitative detail. The surface charge density of the nanopores and the capacitance of the membrane, which are critical determinants of electrokinetic flow through NCA, fall out of the analysis in a natural way, providing a clear mechanism to determine these critically important parameters.

Introduction

Micro total analysis systems (μ-TAS) (Manz et al., 1990) are becoming increasingly significant in chemical and biological sensing, molecular separations, drug delivery and other technologies. (Wakeman and Tarleton, 1991; Van der Schoot et al., 1992; Wooley and Mathies, 1994; Haab and Mathies, 1999; Han and Craighead, 2000; Mitchell et al., 2002) To realize the ultimate promise of μ-TAS it will be crucial to establish communication between different regions of the device where sample concentration, isolation, reaction and detection occur. As an attractive alternative to using mechanical pumps, filters, manifolds and valves in order to achieve fluidic communication between different device zones, molecular gates, constructed from nanocapillary array (NCA) membranes, can be utilized as digital nanofluidic switches. These molecular gates can be optimized for specific functions within the device by adjusting the nanopore diameter, the chemical composition inside the pore

and the applied external bias. (Kemery et al., 1998; Kuo et al., 2001, 2003a,b, 2004; Cannon et al., 2003).

Transport through the cylindrical nanochannels constituting the NCA is governed by the product of the channel diameter, a, and the inverse Debye length, κ. (Kuo et al., 2001 (Langmuir); McDonald et al., 2000) The κa product can be tuned by adjusting κ such that the electrical double layer is either small in relation to the pore diameter ($\kappa a \geq 1$) or more diffuse and spanning the pore ($\kappa a < 1$), by simply adjusting the concentration of electrolyte. When ($\kappa a \gg 1$), flow in the nanopore is dominated by electrophoresis and when ($\kappa a \leq 1$), electroosmotic flow dominates. (Kemery et al., 1998; Kuo et al., 2001 (Langmuir)) By adjusting these parameters and applying an external potential the nanochannel arrays, can be made to behave like digital fluidic switches, and movement of molecules can be controlled with high precision and temporal control.

Although current μ-TAS technology is largely two-dimensional, the obvious analogy to 3D design in VLSI electronics is ample motivation to explore how different areas in the device can achieve fluidic communication, either by receiving sample or delivering it to the next stage in order to sequentially link analytical unit operations. NCA-based molecular gates are well-suited to this application, because: (1) they are simple to integrate into a device as interconnects that transport molecules between microfluidic layers; (2) they can be operated digitally, and, as such, are insensitive to environmental perturbations, since their action is based on an externally applied stimulus; (3) they can be used as vertical interconnects to provide fluidic communication among different regions in a microfluidic device in the same way that metallic vias establish communication among differing levels in VLSI circuitry. Thus, a gateable (externally controllable) fluidic interconnect between microfluidic layers is the critical extension of fluidic circuitry needed to exploit the third dimension and establish fluidic communication among any number of vertically stacked planes containing independently addressable functional layers.

Clearly the κa product is the critical dimensionless parameter which determines the dominant mechanism for nanofluidic transport. It has previously been shown (Kuo et al., 2001 (Langmuir)) that the magnitude of nanofluidic flow can be controlled by adjusting the surface charge density, σ, which, in turn, is directly linked to the magnitude of κ through the requirement for charge neutrality. In addition, the capacitance of the membrane can influence the transient variation of the current through the hybrid micro/nano fluidic structure. Thus, knowledge of how the surface charge density of the nanopores and the capacitance of the membrane couples fluidic motion through a nanocapillary in electrical communication with two microchannels of much larger total volume is critical for design purposes. Yet it is extremely difficult to obtain information about this process for a given nanocapillary or NCA from experiment alone. The work undertaken here seeks to connect phenomena occurring in coupled microchannels and nanocapillaries by exploiting self consistent modeling and simulations to reproduce, in quantitative detail, the electrical behavior of the coupled microfluidic and nanofluidic transport phenomena, thereby yielding powerful new insights into the behavior of these nanofluidic–microfluidic hybrid architectures.

Theory and mathematical models

The physical model for the nanofluidic–microfluidic hybrid architecture is shown in Figure 1, and the impedance network model for the combined

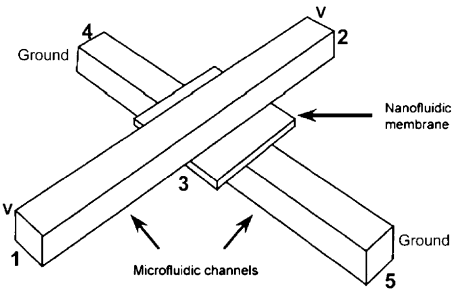

Figure 1. Schematic diagram of crossed microfluidic channels separated by a nanoporous membrane. The top μ-fluidic channel (1–2) is designated the receiving channel and the bottom μ-fluidic channel (4–5) the source channel. The dimensions of the microfluidic channels are 14 mm × 100 μm (wide) × 60 μm (deep). During the analysis of flow through the hybrid device, a positive electrical potential, $V_1 = V_2$, is applied at the ends of the receiving channel (top microfluidic channel), and the ends of the source channel (bottom microfluidic channel) are grounded, $V_4 = V_5 = 0$.

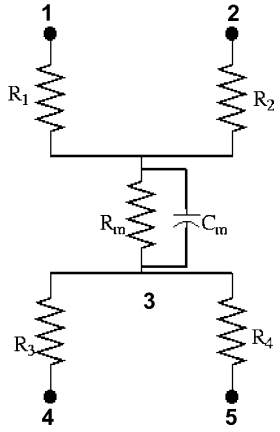

Figure 2. The electrical circuit model representation of the hybrid nanofluidic–microfluidic device.

microfluidic and nanofluidic channels is shown in Figure 2. R_1 and R_2 represent the electrical resistances of the two segments in the receiving channel, and R_3 and R_4 those of the comparable segments in the source channels. The combined electrical resistance of the nanochannels in the membrane is represented by R_m. The capacitance of the membrane, C_m, is considered when modeling the transient variation of the electrical current.

In this section we present the mathematical model to compute the resistances of the microfluidic channels (R_{1-4}), the mathematical models to compute the resistance of the membrane are presented, the model to estimate the capacitance of the membrane, and the mathematical models for transient analysis.

Resistance of microfluidic channels

To simulate current through the electrical circuit shown in Figure 2, a compact model (Qiao and Aluru, 2002; Chatterjee and Aluru, 2005) is used to compute the resistance of the microfluidic channel segments (i.e. R_{1-4}). The electrical current density, J, through a fluidic channel is given by the expression, (Probstein, 1994)

$$J = F\sum_{i=1}^{N} z_i \Gamma_i \tag{1}$$

where F is the Faraday's constant, N is the total number of ionic species, z_i is the valence of the ith species and Γ_i is the axial component (along the direction of the electric field) of the flux of the ith species. The axial flux of the ith species is given by the expression, (Oldham and Myland, 1994)

$$\Gamma_i = -D_i\frac{\partial c_i}{\partial x} - \mu_i z_i F c_i \frac{\partial \Phi}{\partial x} + c_i u \tag{2}$$

where D_i is the diffusion coefficient, μ_i the ionic mobility, and c_i the concentration of the ith species, u is the axial velocity of the bulk flow, and is the electrical potential. The Einstein relationship (Probstein, 1994) relates the ionic mobility to the diffusion coefficient,

$$\mu_i = D_i/RT \tag{3}$$

where R is the universal gas constant and T is the absolute temperature. The electrical potential, Φ; can be represented as the sum of two components,

$$\Phi = \phi + \psi \tag{4}$$

where ϕ is the electrical potential due to the externally applied electrical field, and ψ is the electrical potential due to the surface charge distribution on the channel wall.

When the flow is electrically driven, the total flux consists of three terms: a diffusional component resulting from the concentration gradient, an electrophoretic component, which stems from the electrical potential gradient, and an electroosmotic component which originates from the non-zero body force acting within the electrical double layer. Typically, the contributions of the diffusional flux and the electroosmotic flux to the net current through a microchannel are negligible. As a result, the electrophoretic flux is the dominant term in the expression for current. Thus, from Eqs. (1) and (2) the expression for the current, I, through the microfluidic channel is given by

$$I = \frac{\Delta\phi}{L}A\left(\sum_{i=1}^{N} z_i^2 F^2 \mu_i c_i\right) = \frac{\Delta\phi}{L}A\sigma \tag{5}$$

where L is the length of the channel, A is the cross-sectional area of the channel, $\Delta\phi$ is the electrical potential drop across the ends of the channel, and σ is the electrical conductivity of the buffer in the channel. Thus, the electrical resistance of the microfluidic channel is given by

$$R = \frac{L}{\sigma A} \tag{6}$$

Equation (6), which is used to compute the resistance of the microfluidic channel, is known as the compact model (Qiao and Aluru, 2002; Chatterjee and Aluru, 2005).

Resistance of the membrane

The resistance models discussed in the previous section (i.e. the compact models) provide good accuracy for the microfluidic channels, since the electrical double layer thickness (of the order of nanometers) is negligible compared to the depth or width of the microfluidic channels. However, such a simple resistance model may not be sufficiently accurate for nanochannels, where the electrical double layer (EDL) thickness can be comparable to the characteristic dimension of the channel. Therefore, the flow through the nanochannels embedded in the membrane is simulated using a full-scale approach requiring a self-consistent solution of the Poisson equation, the Nernst–Planck equation and the Navier–Stokes equations. (Oldham and Myland, 1994) The electrical potential distribution is governed by the Poisson equation

$$\nabla^2\Phi = -\frac{\rho_e}{\varepsilon_0\varepsilon_r} \tag{7}$$

where ε_0 is the permittivity of free space and ε_r is the dielectric constant of the medium. For an electrolyte, the net charge density, ρ_e, is given by,

$$\rho_e = F\sum_{i=1}^{N} z_i c_i \tag{8}$$

The Nernst–Planck equation defines the molar flux density of the ith ionic species (Eq. (2)), which includes the flux due to diffusion, electrical migration and convection. At steady-state, the conservation of flux leads to the continuity equation

$$\nabla \cdot \Gamma_i = 0 \tag{9}$$

where Γ_i is defined in Eq. (2). The Navier–Stokes equations, describing the fluid flow through the channel, are given by (White, 2002),

$$\eta\nabla^2\mathrm{u} - \nabla p - \rho_e\nabla\Phi = 0 \tag{10}$$

and

$$\nabla\bullet\mathrm{u} = 0 \tag{11}$$

where p is the fluidic pressure and η is the dynamic viscosity of the fluid. The third term in Eq. (10) represents the body force due to the electrical potential gradient acting on the net charge density.

The Poisson equation, Eq. (7), the Nernst–Planck equation, obtained by combining Eqs. (2) and (9), and the Navier–Stokes equations, Eqs. (10) and (11), are all coupled to each other. Hence, an iterative process is used to compute a self-consistent solution. Using an initial guess for the convective velocity, the concentration of the ions and the electrical potential are computed from the coupled Poisson and Nernst–Planck (PNP) equations by using the Newton–Raphson scheme. Using the concentration of the various ions and the potential gradient computed from the PNP equations, the Navier–Stokes equations are solved to compute the velocity vector. The PNP and the Navier–Stokes equations are solved iteratively until a self-consistent solution for the concentration of the ions, electrical potential and the velocity is obtained. A relative tolerance of 10^{-5} has been used for ensuring the convergence of the coupled equations. Finally, the flux of the various ionic species and the net current through the fluidic channel are computed by using Eqs. (2) and (1), respectively. Thus, for a given applied electrical potential, we compute the corresponding current through the membrane. The resistance of the membrane is extracted as the inverse of the slope of the I–V (current versus voltage) plot generated from the full-scale simulations corresponding to different electrical potentials applied across the membrane. The CPU time to compute the IV plots is of the order of several minutes on a 2.4 GHz processor.

Capacitance of the membrane

In general, charge in the capacitor is stored at the surface of the electrodes. However, polymer based capacitors store charge throughout the volume due to the presence of fixed charged groups. Therefore, the capacitance of the polymeric membrane cannot be computed by using the typical expression for a parallel plate capacitor. Application of a potential difference across the polymer leads to migration of ions, which tends to neutralize the charged groups. Thus, the capacitance of the membrane can be estimated by

$$C_m = \frac{c_f \times F \times V_{m-p}}{\Delta\phi} \tag{12}$$

where c_f is the concentration of the fixed charged group in the membrane, V_{m-p} is the volume of the membrane excluding the volume of the pores, and $\Delta\phi$ is the electrical potential drop across the membrane, which can be computed from the impedance model during the steady-state analysis. The value of c_f for the membranes used here is not known precisely and typically the concentration of the fixed charged group can range from a few milli Molar (Chun et al., 2002) to a few Molar (the manufacturer (Osmonics (Minnetonka, MN)) of the membrane suggested that a reasonable value for c_f is 1 M). Similarly, the precise value for V_{m-p} is also difficult to compute. Typically, V_{m-p} is obtained from the overlap region between the microfluidic channels and the membrane. However, once the ions enter the membrane though the overlap region, they can diffuse into regions outside of the overlap region to compensate the fixed charged group. This is also evidenced by the fact that in some experiments the membrane was found to be leaky. As a result, the value of V_{m-p} (for the 6 μm thick membrane and 15 nm diameter pores) can vary from 6×10^{-5} mm^3 to 6×10^{-2} mm^3. Given the uncertainty in c_f and V_{m-p}, the product of c_f and V_{m-p} can vary from 0.3 milli moles to 300 moles, which gives rise to a capacitance variation of 1.4 nF to 1.4 mF. In our calculations, we found that a C_m of 3 μF gives the best match with the experimental data. If we assume $c_f = 1$ M, a C_m of 3 μF suggests that the volume, V_{m-p}, that should be used to calculate the capacitance of the membrane is slightly larger than the overlap region. On the other hand, if we assume that V_{m-p} is the overlap region, then a capacitance of 3 μF for the membrane suggests that $c_f = 10.9$ M.

Transient analysis

To understand the mechanism for the transient variation of current through the hybrid device, consider Figure 1, where a positive electrical potential is applied at the ends of the receiving channel (top microfluidic channel in Figure 1), which serves as the anode. The ends of the source channel (bottom microfluidic channel in Figure 1) are grounded and serve as the cathode. Consider the case of a membrane with a negative fixed wall charge, e.g. from deprotonated carboxylic acid surface moieties. Initially, as the external electrical field is applied, the cations having a higher electrophoretic mobility migrate preferentially inside the membrane to neutralize the charged membrane, thus creating a capacitance effect. As the fixed groups in the membrane are negatively charged, it is energetically favorable for the cations, and energetically unfavorable for the anions, to enter the nanopores. Therefore, the slower anions tend to stack outside the nanopores. The current through the receiving channel during this phase can be modeled using an RC circuit as shown in Figure 2. (Lurch, 1971) For simplicity, we consider the portion of the device that includes the membrane and the receiving channel, i.e. from node 3 upward to nodes 1 and 2 in Figure 2. Therefore, the corresponding circuit includes the resistance of the membrane (R_m), the capacitance of the membrane (C_m) and the resistances of the receiving channel segments (R_1 and R_2). Assuming the potential drop between the anode and the junction of the membrane and the source channel is ΔV, the variation of current with time through the receiving channel is given by

$$I(t) = \frac{\Delta V}{R_{\text{eq}}}\left[1 - \exp\left(\frac{-t}{R_{\text{eff}}C_m}\right)\right] \tag{13}$$

where R_{eff} and R_{eq} are given by the expressions,

$$R_{\text{eff}} = \frac{R_m(R_1R_2/(R_1 + R_2))}{R_m + (R_1R_2/(R_1 + R_2))} \tag{14}$$

and

$$R_{\text{eq}} = R_m + R_1R_2/(R_1 + R_2) \tag{15}$$

At the end of the charging phase, the fixed charges of the membrane have been shielded by the cations. The stacked anions then migrate through the nanochannels due to the electrical potential gradient. The transport of the ions can be modeled by using the transient Nernst–Planck equation (Probstein, 1994). Thus, the spatial concentration profile of the ionic species and the corresponding conductivity profile can be updated at every time step by adding the effect of the anion migration. Finally, a steady-state is reached when the concentration profile and the current do not change with time.

Experimental

Device fabrication

The three dimensional transport device was fabricated by techniques described previously. (Kuo et al., 2003a, b) The microfluidic channels were fabricated in poly(dimethoxysiloxane), PDMS, using standard rapid prototyping protocols for PDMS (McDonald et al., 2000). To assemble the device a 10 mm × 1 mm section of a track-etched polycarbonate (PCTE) membrane (30 nm pore diameter) was centered on the bottom of a PDMS channel and the top channel was placed at 90° to the bottom channel within the area of the membrane. The thickness of the membrane is 6 μm when the pore diameter is 30 nm and 15 nm, and 10 μm when the pore diameter is 200 nm. There are 60×10^3 pores in the gate area for the membranes with 15 and 30 nm diameter pores, and 7500 pores in the gate area for the membranes with 200 nm diameter pores. The membranes are obtained from Osmonics (Minnetonka, MN). To facilitate sealing, the PDMS was treated with an O_2 plasma. (Cannon et al., 2003). The channels used in the experiments were 100 μm wide, 60 μm deep and 14 mm long. A reservoir PDMS layer was sealed onto the top of the sandwich structure to complete the device.

Electrical characterization

Ohm's law plots were obtained by recording the current at a given voltage across a single layer channel, while the other layer microchannel was electrically floated. The measurements were done rapidly to avoid significant amounts of electroosmotic flow. All measurements were performed after preconditioning the membrane at 20 V for a ~5 min. The current was recorded by measuring the voltage across a 100 kΩ resistor using a Keithley nanovoltmeter interfaced to a specially written Labview (National Instruments) collection program. Voltages were applied to the microchannels through a computer-controlled (Labview) 8-relay system. (Cannon et al., 2003).

Transient analysis experiments

To obtain transient transport data both device channels were filled with 10 mM phosphate buffer solution, sodium salt, pH 7.4. A 40-V symmetrical bias was applied for all transport configurations. To do this the source channel was grounded at both ends, while the positive voltage was applied to both ends of the receiving channel. The configuration was quickly switched in the relay system by applying the voltage in the source channel and grounding the receiving channel. The current was recorded by measuring the voltage across a 100 kΩ resistor using a Keithley nanovoltmeter interfaced to a Labview collection program.

Results and discussion

First, we present the results obtained from steady-state simulation, and then the transient simulation results are presented. Flow through the microfluidic channels is simulated using the model presented in Eqs. (7)–(12). Phosphate buffer of constant composition (6 mM of Na_2HPO_4:4 mM NaH_2PO_4) is used in all the simulations. The following diffusivities were used: $D_{Na^+} = 1.334 \times 10^{-9} m^2/s$, $D_{HPO_4^{2-}} = 0.439 \times 10^{-9} m^2/s$, and $D_{H_2PO_4^-} = 0.879 \times 10^{-9} m^2/s$. (Berry et al., 1980). The surface charge density of the nanopore was not known *a priori*. We used a value of $\sigma = -2 \times 10^{-3}$ C/m^2 in all the simulations, which provided good agreement between the experimental and simulation results. This surface charge density is within a factor of two of the value reported for a similar membrane. (Letmann et al., 1999).

Figure 3 shows the I–V plot for the microfluidic channel filled with phosphate buffer. The dimensions of the channel are given in the caption of Figure 1. The simulation results and the experimental results compare well, validating the use of the computationally inexpensive compact model for computing the resistance of the microchannels of the hybrid nano/microfluidic device.

Figure 4 shows a similar I–V plot for a nanofluidic membrane comprised of 30 nm diameter pores. Note that the current is for the entire membrane (gate area) and not for a single pore. The simulated I–V curve compares well with the experimental results. In calculations, we have first computed the current through a single pore and

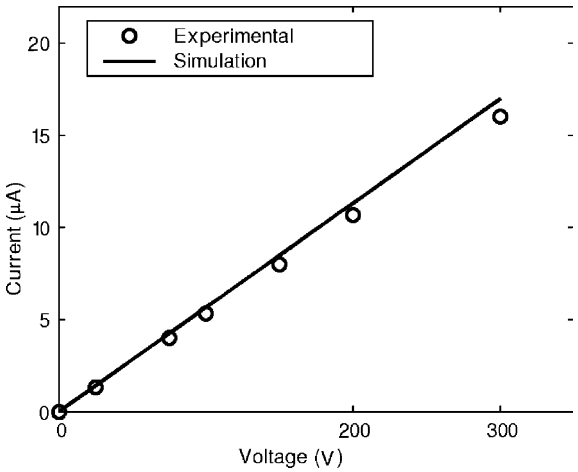

Figure 3. Plot of the I–V relationship for the microfluidic channel obtained from the ohmic compact model (solid line) compared to experimental results (open circles).

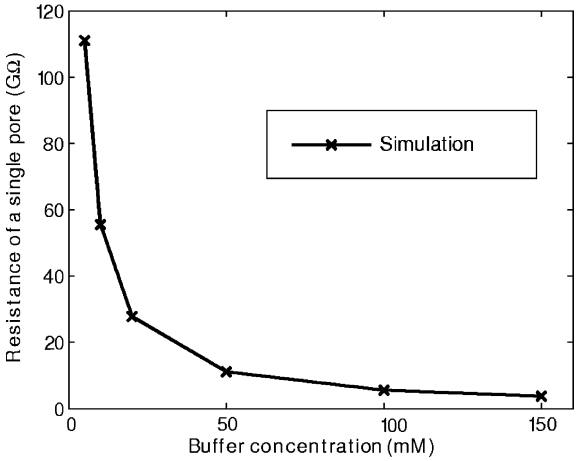

Figure 5. Effect of the concentration of the buffer on the resistance of a single 200 nm diameter pore obtained using the full-scale simulation.

multiplied it by the number of pores to get the current through the membrane. The resistance of a single pore and the membrane can be computed from inverse of the slope of the I–V curves for the single pore and the membrane, respectively. The resistance of a single nano-pore is expected to vary in a non-linear fashion with the diameter of the pore and the buffer concentration, and the model recovers this behavior, as shown in Figures 5 and 6. These results indicate that the size of the pore and the buffer composition can be utilized as important device parameters for tuning the resistance of the membrane and of the hybrid nano/microfluidic device.

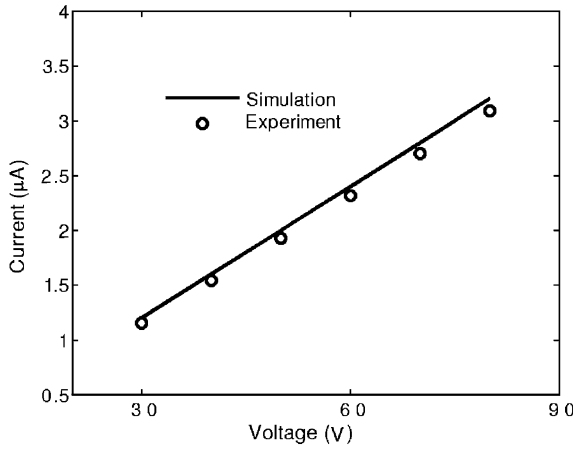

Figure 4. I–V plot for the nanocapillary membrane obtained using the full-scale simulation for 10 mM phosphate buffer and 30 nm pore diameter. The resistance of the membrane extracted from the I–V plot is 24.67 MΩ.

Figures 7 and 8 show the transient variation of the electrical current as measured in the receiving or the source microchannel upon application of a forward bias potential to the nanocapillary membrane. The behavior is, in general, much more complicated than one might be led to expect based on the simple equivalent circuit of Figure 2. Neither side exhibits a simple exponential behavior, however the experimental behavior is recovered in quantitative detail by the self-consistent solutions to the coupled Poisson, Nernst–Planck and Navier–Stokes equations.

The transient behavior can be understood by breaking the transport conceptually into discrete time windows. First, consider the receiving channel. During the charging phase, $0 < t < 25$ s in Figure 7, the capacitance effect is observed as the cations, with higher ionic mobility, migrate preferentially through the nanocapillaries. During this process, the slow moving anions lag behind. The overall current in the receiving channel increases in this phase due to the increase in total ion content of the plug adjacent to the NCA membrane. In the next phase, $t > 25$ s in Figure 7, as the anionic species are transported through the nanocapillaries to the receiving microchannels, the effective electrical conductivity in the receiving microchannel

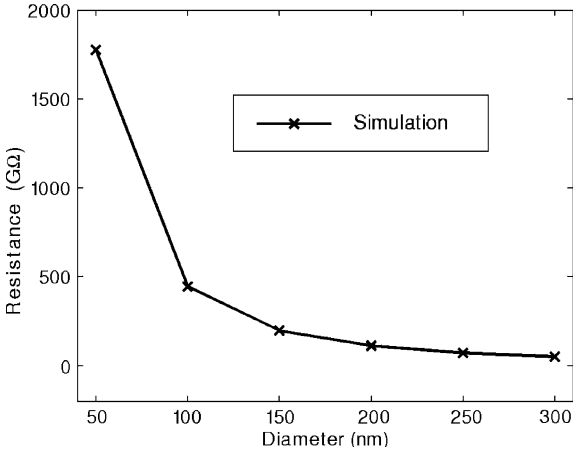

Figure 6. Effect of the diameter of the nanopore on the resistance of a single pore obtained using the full-scale simulation. The buffer concentration is 5 mM.

increases more, and the electrical current measured in the receiving channel increases until a steady-state is reached. It is notable that the simulation reproduces the qualitative and quantitative behavior of the receiving channel current and that the critical parameters in determining the quantitative agreement are the capacitance of the membrane, C_m, and the surface charge density, σ. Given the inherent difficulty of performing streaming potential measurements for nanocapillary array membranes under these conditions, the self-consistent modeling approach gives a very nice route to recover these fundamentally important parameters for nanochannel electrokinetic transport.

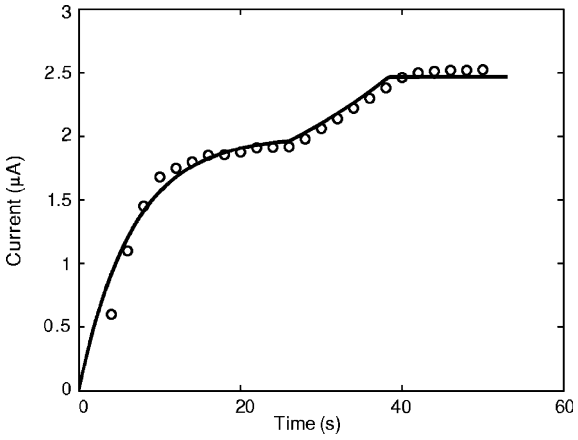

Figure 7. Comparison of experimental (open circles) and simulation (solid line) results for the microchannel current on the receiving (anode) side of a 15 nm pore diameter membrane in 10 mM phosphate buffer at pH 7.4. Forward bias is applied at $t = 0$.

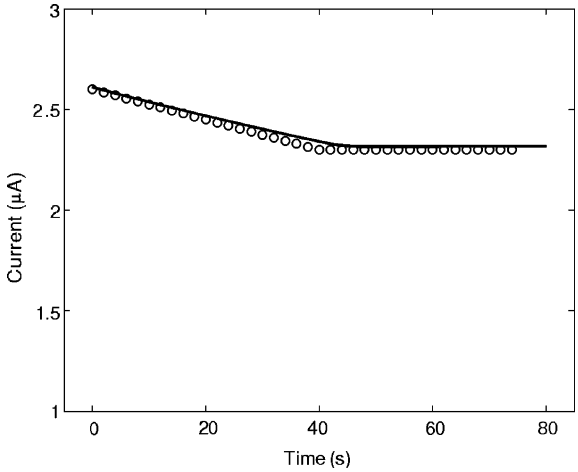

Figure 8. Comparison of experimental (open circles) and simulation (solid line) results for the microchannel current on the source (cathode) side of a 15 nm pore diameter membrane in 10 mM phosphate buffer at pH 7.4. Forward bias is applied at $t = 0$.

The opposite effect is observed in the source channel with one important difference. Because the experiment and simulation target a 15 nm pore diameter nanocapillary membrane and because the bias voltage is not large enough to saturate transport through the membrane, the magnitude of the effect is much smaller in the source channel. As the anionic species migrate away, the electrical conductivity and the electrical current decrease before a steady-state is reached. Steady state is reached in the source channel at approximately the same time delay as that in the receiving channel, adding further confidence that the simulations are reproducing the nanofluidics correctly.

To further understand the effect of the capacitance of the membrane and the surface charge density on nanofluidic transport, we have performed current versus time calculations on the 15 nm diameter pore membrane by varying the capacitance of the membrane and the surface charge density.

Figure 9 shows the variation in the current versus time profile for three different capacitances of

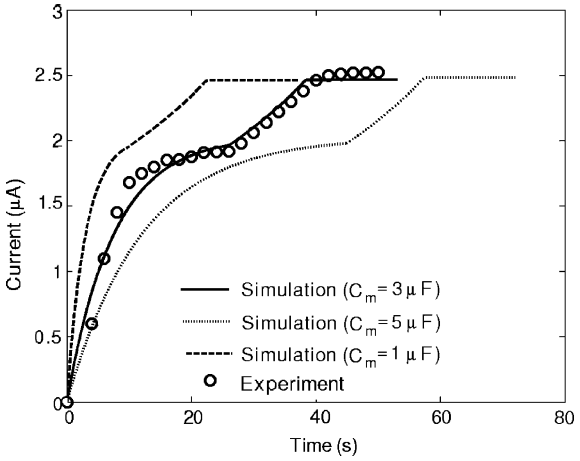

Figure 9. The variation in the current versus time profile for three different capacitances of the 15 nm diameter pore membrane. The surface charge density is -0.002 C/m^2.

the membrane. While the steady-state current is independent of the capacitance of the membrane, the time to reach steady-state can increase with the increase in capacitance. For a lower capacitance, the charge in the membrane can be shielded quickly by the cations and the anions stacked outside the nanopore can enter the nanopore sooner when compared to a larger capacitance membrane.

Figure 10 shows the variation in the current versus time profile for three different surface charge densities of the nanopore. We observe that a larger surface charge density gives rise to a higher steady-state current and the time to reach steady-state is weakly dependent on the surface charge density.

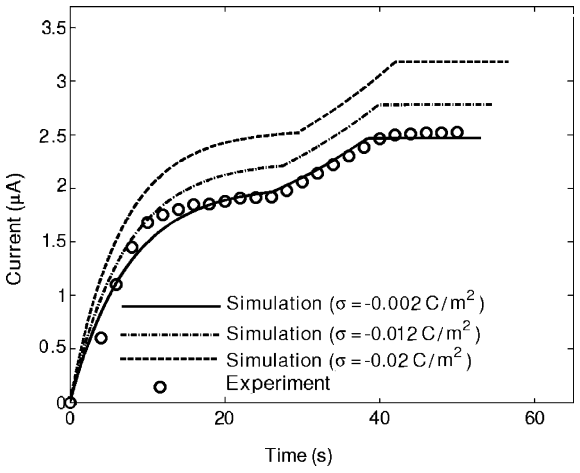

Figure 10. The variation in the current versus time profile for three different surface charge densities for the 15 nm diameter pore membrane. The capacitance of the membrane is 3 μF.

Conclusions

The technological drivers pushing development of multi-dimensional, i.e. sequential, methods of processing and chemical analysis demand the development of three-dimensional architectures to realize their full potential. Accessing the third dimension requires a mechanism of digital fluidic switching that allows communication among vertically separated independent planar processing areas, and the NCA membranes being studied in this laboratory provide a powerful and facile method of accomplishing this digital fluidic switching. However, the use of structures which utilize both micro- and nanoscale phenomena raises new questions about the fundamental physical factors which control fluid motion. While compact models can reproduce microscale electrical behavior, the nanoscale phenomena require self-consistent solutions of the coupled electrical and fluid flow equations. The work presented here demonstrates that these self consistent solutions can reproduce the nanoscale behavior, even in cases where the temporal development of steady state behavior is quite complicated. In addition, the surface charge density and the capacitance of the membrane, which are critical parameters for electrokinetic flow in hybrid micro/nano-fluidic control structures, falls out of the analysis in a natural way, providing a clear mechanism to determine these critically important, but experimentally intractable parameters. Knowledge of the absolute magnitude of σ can be used to understand the manner in which processing and solution conditions can be used to manipulate σ and, therefore, the mechanism of nanofluidic flow under a given set of conditions. Beyond the specific results presented here we envision that the approaches developed here may be extended to more complicated arrangements of micro- and nanoscale fluidic control structures and that the interplay between calculation and experiment will continue

to be fruitful in increasing our understanding of the behavior of these novel structures.

Acknowledgments

This work was supported by the National Science Foundation through the Science and Technology Center for Advanced Materials for Water Purification, and the Nano-CEMMS center (under grant No. 0328162), and by the Department of Energy under grant DE FG02 88ER13949.

References

Berry R.S., S.A. Rice & J. Ross, 1980. Physical Chemistry. New York: John Wiley Sons.

Cannon D.M., T.-C. Kuo, P.W. Bohn & J.V. Sweedler, 2003. Nanocapillary array interconnects for gated analyte injections and electrophoretic separations in multilayer microfluidic architectures. Anal. Chem. 75, 2224–2230.

Chatterjee A.N. & N.R. Aluru, 2005. Combined circuit/device modeling and simulation of integrated microfluidic systems. J. Microelectromech. Sys. 14, 81–95.

Chun K.-Y. & P. Stroeve, 2002. Protein transport in nanoporous membranes modified with self-assembled monolayers of functionalized thiols. Langmuir 18, 4653–4658.

Haab B.B. & R.A. Mathies, 1999. Single-molecule detection of DNA separations in microfabricated capillary array electrophoresis chips employing focused molecular streams. Anal. Chem. 71, 5137–5145.

Han J. & H.G. Craighead, 2000. Separation of long DNA molecules in a microfabricated entropic trap array. Science 288, 1026–1029.

Kemery P.J., J.K. Steehler & P.W. Bohn, 1998. Electric field mediated transport in nanometer diameter channels. Langmuir 14, 2884–2889.

Kuo T.-C., H.K. Kim, D.M. Cannon, P.W. Bohn & J.V. Sweedler, 2004. Nanocapillary arrays effect mixing and reaction in multilayer fluidic structures. Angew. Chem. Int. Ed. 43, 1862–1865.

Kuo T.-C., D.M. Cannon, Y.N. Chen, J.J. Tulock, M.A. Shannon, J.V. Sweedler & P.W. Bohn, 2003a. Gateable nanofluidic interconnects for multilayered microfluidic separation systems. Anal. Chem. 751861–1867.

Kuo T.-C., D.M. Cannon, M.A. Shannon, P.W. Bohn & J.V. Sweedler, 2003b. Hybrid three-dimensional nanofluidic/Microfluidic devices using molecular gates. Sensons Actuators A 102, 223–233.

Kuo T.-C., D.M. Cannon Jr., W. Feng, M.A. Shannon, J.V. Sweedler & P.W. Bohn, 2001. Three-dimensional fluidic architectures using nanofluidic diodes to control transport between microfluidic channels in microelectromechanical devices. Micro Total Analysis Systems 2001, Monterey CA, USA. October 2001, 60–62.

Kuo T.-C., L.A. Sloan, J.V. Sweedler & P.W. Bohn, 2001. Manipulating molecular transport through nanoporous membranes by control of electrokinetic flow: Effect of surface charge density and Debye length. Langmuir 17, 6298–6303.

Lettmann C., D. Mockel & E. Staude, 1999. Permeation and tangential flow streaming potential measurements for electrokinetic characterization of track-etched membranes. J. Membr. Sci. 159, 243–251.

Lurch E.N., 1971. Fundamentals of Electronics. John Wiley & Sons.

Manz A., N. Graver & H.M. Widmer, 1990. Miniaturized total chemical analysis systems-a novel concept for chemical sensing. Sens. Actuat. B. 1, 244–248.

Mitchell D., S. Bok Lee, L. Trofin, N. Li, K. Nevanen, H. Söderlund & C. Martin, 2002. Smart nanotubes for bioseparation and biocatalysis. J. Am. Chem. Soc. 124, 11864–11865.

McDonald J.C., D.C. Duffy, J.R. Anderson, D.T. Chiu, H.K. Wu, O.A. Schueller & G.M. Whitesides, 2000. Fabrication of microfluidic systems in poly(dimethylsiloxane). Electrophoresis 21, 27–40.

Oldham K.B. & J.C. Myland, 1994. Fundamentals of Electrochemical Science. San Diego: Academic Press Inc.

Probstein R.F., 1994. Physiochemical Hydrodynamics. New York: Wiley.

Qiao R. & N.R. Aluru, 2002. A compact model for electroosmotic flows in microfluidic devices. J. Micromech. Microeng. 12, 625–635.

Vander Schoot B.H., S. Jeanneret, A. Berg & N.F. Rooij, 1992. A silicon integrated miniature chemical analysis system. Sensors Actuators B 6, 57–60.

Woolley A.T. & R.A. Mathies, 1994. Ultra-high-speed DNA fragment separations using microfabricated capillary array electrophoresis chips. Proc. Natl. Acad. Sci. USA 91, 11348–11352.

Wakeman R.J. & E.S. Tarleton, 1991. An experimental-study of electro-acoustic cross flow microfiltration. Chem. Eng. Res. Des. 69, 386–397.

White F.M., 2002. Fluid Mechanics. McGraw-Hill.